This is the accepted manuscript made available via CHORUS. The article has been published as:

Electron and hole transport in disordered monolayer MoS_{2}: Atomic vacancy induced short-range and Coulomb disorder scattering

Kristen Kaasbjerg, Tony Low, and Antti-Pekka Jauho

Phys. Rev. B **100**, 115409 — Published 6 September 2019

DOI: 10.1103/PhysRevB.100.115409

Electron and hole transport in disordered monolayer MoS_2: atomic vacancy-induced short-range and Coulomb disorder scattering

Kristen Kaasbjerg,[1,*] Tony Low,[2] and Antti-Pekka Jauho[1]

[1] *Center for Nanostructured Graphene (CNG), Department of Physics, Technical University of Denmark, DK-2800 Kongens Lyngby, Denmark*
[2] *Department of Electrical and Computer Engineering, University of Minnesota, Minneapolis, MN 55455, USA*

(Dated: August 26, 2019)

Atomic disorder is a common limiting factor for the low-temperature mobility in monolayer transition-metal dichalcogenides (TMDs; MX_2). Here, we study the effect of often occuring atomic vacancies on carrier scattering and transport in p- and n-type monolayer MoS_2. Due to charge trapping in vacancy-induced in-gap states, both *neutral* and *charged* vacancies resembling, respectively, short-range and combined short-range and long-range Coulomb scatterers, must be considered. Using the T-matrix formalism, we demonstrate a strong renormalization of the Born description of short-range scattering, manifested in a pronounced *reduction* and a characteristic energy dependence of the scattering rate. As a consequence, carrier scattering in TMDs with charged vacancies is dominated by the long-range Coulomb-disorder scattering, giving rise to a strong screening-induced temperature and density dependence of the low-temperature carrier mobility. For TMDs with neutral vacancies, the absence of intrinsic Coulomb disorder results in significantly higher mobilities as well as an unusual density dependence of the mobility which *decreases* with the carrier density. Our work illuminates the transport-limiting effects of atomic-vacancy scattering relevant for high-mobility TMD devices.

I. INTRODUCTION

Two-dimensional (2D) monolayers of transition metal dichalcogenides (TMDs; MX_2) hold great promise for future electronics and optoelectronics.[1–4] In addition, their spin-valley coupling[5,6] makes them potential candidates for spin- and valleytronics applications, which among other things has sparked interest in TMD-based quantum-dot qubits.[7–11] For such purposes, high-mobility samples with long spin and valley life times are essential.

Like in conventional 2D semiconductor heterostructure systems, disorder sets the ultimate limit for the achievable low-temperature mobility in monolayer TMDs,[12] most often limited by short-range and Coulomb disorder scattering.[13–21] Only recently have mobilities exceeding $\sim 1000\ \mathrm{cm^{-2}\,V^{-1}\,s^{-1}}$ been achieved.[11,22–25]

On the theoretical side, studies of the transport properties have focused on semiclassical transport including electron-phonon[26–29] and charged impurity scattering,[30,31] microscopic descriptions of atomic point defects within the Kubo formalism,[32–34] and quantum-transport studies.[34–41] However, the impact of atomic disorder on the transport properties is still poorly understood.

In experimental STM studies on monolayer TMDs, atomic monovacancies have been found to be among the dominating sources of intrinsic lattice disorder.[43–48] Their stability and electronic structure have been studied in great detail theoretically,[49–57] demonstrating that they often introduce in-gap states, as illustrated in Fig. 1 for a S vacancy in MoS_2, which are localized at the vacancy site. In-gap states play a crucial role in the transport properties of 2D TMDs as they can trap charges. At low gate-induced doping levels, electrons become trapped in empty in-gap states and variable-range hopping between the defect sites dominates the transport.[16,58–61] With increasing doping, the material becomes n-type with free carriers in the conduction band. At this point, a transition from the insulating state with thermally-activated hopping transport to a metallic conduction regime with a conductivity (resistivity) that decreases (increases) with increasing temperature takes place.[13,14,16,17,58,62–64] Usually, metallic behavior is attributed to electron-phonon scattering, but this is suppressed at low temperature and disorder scattering by, e.g., atomic vacancies becomes the mobility-limiting factor.[16–20]

In this work, we provide an in-depth study of the effect of atomic vacancies on carrier scattering and transport in p- and n-type 2D MoS_2. Conventionally, atomic vacan-

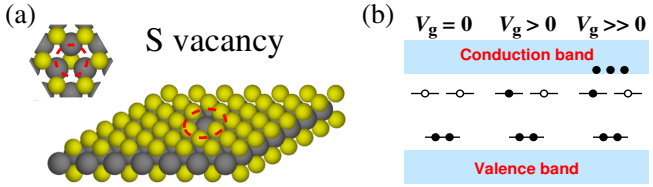

FIG. 1. Atomic vacancies in 2D TMDs. (a) Top and side views of the atomic structure of a sulfur vacancy in 2D MoS_2. The C_{3v} symmetry of the vacancy site results in a protection against intervalley scattering.[42] (b) Sulfur vacancy-induced in-gap states. In the undoped material ($V_g = 0$), the state close to the valence band maximum is occupied with two electrons from the missing sulfur anion. With an applied gate voltage, $V_g > 0$, one electron is trapped in the upper in-gap states before carriers are introduced into the conduction band ($V_g \gg 0$).

cies in 2D TMDs are treated as *neutral* point defects (see, e.g., Ref. 33) which act as short-range scatterers. However, in the presence of vacancy-induced in-gap states, vacancies may acquire a dual character due to charging of the vacancy site, and should be treated as combined short-range and long-range Coulomb (i.e., charged impurity) scatterers.

The situation for an S vacancy in 2D MoS_2[49–57] is illustrated in Fig. 1 where the vacancy gives rise to three in-gap states. The lowest state is doubly occupied in the undoped, charge neutral material ($V_g = 0$), and hence behaves as a donor state which traps holes in p-doped materials. On the other hand, the upper states are empty and behave as deep single-electron acceptors which trap electrons in n-doped ($V_g > 0$) samples[16,50,51,59] (doubly charged vacancy sites are expected to be prohibited by a large onsite Coulomb repulsion energy). Thus, S vacancies are expected to acquire a net charge in p- or n-doped MoS_2 (positive and negative, respectively) due to charging of the in-gap states. The same holds for Mo vacancies in MoS_2 (see, e.g., Ref. 55). However, while vacancies in 2D TMDs, in general, seem to introduce empty in-gap states, occupied states above the valence-band edge are not always present.[55,65] In the latter case, the vacancy will remain neutral in the p-doped material.

Based on the T-matrix formalism,[66,67] we here demonstrate that the scattering amplitude for the short-range component of the scattering potential is strongly renormalized with respect to its value in the Born approximation. For charged vacancies, this renders the short-range potential irrelevant in comparison to the Coulomb contribution to the scattering potential, and effectively reduces the vacancies to charged impurities.

The dominance of Coulomb disorder scattering gives rise to a strong temperature and density dependence of the mobility which stems from the temperature dependent screening of the Coulomb potential. In the degenerate low-temperature ($T \ll T_F$) regime, Coulomb disorder resembles short-range disorder due to the efficient carrier screening in 2D TMDs, and yields a $\mu \sim n^0, T^0$ behavior. At the crossover to the nondegenerate ($T \gtrsim T_F$) regime, the screening efficiency is strongly reduced due to the temperature dependence of the 2D screening function, and the experimentally observed metallic behavior with a mobility that decreases with increasing temperature and increases with the carrier density prevails. While this behavior is inherent to any 2D semiconductor systems at the quantum-classical crossover ($T = T_F$) between the degenerate and nondegenerate regimes,[68] the temperature and density interval where the crossover takes place is highly dependent on material parameters (spin and valley degeneracy, effective mass). For typical carrier densities (10^{11}–10^{13} cm^{-2}) in 2D TMDs, the Fermi temperature falls in the range $1\,\mathrm{K} \lesssim T_F \lesssim 100\,\mathrm{K}$, thus placing the quantum-classical crossover in an easily accessible temperature range where phonon scattering is weak.[26,27]

In 2D TMDs where the vacancies remain *neutral* in the p-doped material, the mobility is demonstrated to be significantly higher and shows much weaker temperature dependence as well as a qualitatively different density dependence with a mobility that *decreases* with the carrier density. This behavior is inherent to atomic-vacancy limited transport in 2D TMDs with charge-neutral vacancies.

Our findings are of high relevance for the understanding of the microscopic factors governing the mobility, magneto and quantum transport in 2D TMDs.[11,19–25,69–71]

II. LOW-ENERGY HAMILTONIAN AND BOLTZMANN TRANSPORT THEORY

In 2D TMDs, the K, K' valence and conduction band valleys illustrated in Fig. 2, can be described by the effective low-energy Hamiltonian[5]

$$\mathcal{H}_\tau(\mathbf{k}) = at\left(\tau k_x \hat{\sigma}_x + k_y \hat{\sigma}_y\right) + \frac{\Delta}{2}\hat{\sigma}_z + \tau\frac{\Delta_{\mathrm{SO}}}{2}\frac{\hat{\sigma}_0 - \hat{\sigma}_z}{2} \otimes \hat{s}_z, \tag{1}$$

where a is the lattice parameter, t a hopping parameter, $\tau = \pm 1$ is the K, K' valley index, Δ is the band gap, Δ_{SO} ($= 148$ meV in 2D MoS_2) is the spin-orbit (SO) induced spin splitting at the top of the valence band,[72] and $\hat{\sigma}_i$, $\hat{\tau}_i$ and $\hat{s}_i$, are the identity ($i = 0$) and Pauli matrices ($i = x, y, z$) in the symmetry-adapted orbital basis, valley and spin, respectively. The orbital basis $\{|\phi_{\sigma\tau}\rangle\}$ is spanned by the M d-orbitals $|\phi_{v\tau}\rangle = 1/\sqrt{2}\left(|d_{x^2-y^2}\rangle + i\tau|d_{xy}\rangle\right)$ and $|\phi_{c\tau}\rangle = |d_{z^2}\rangle$.

In the continuum description of Eq. (1), the wave function can be expressed as (suppressing the spin index $s = \pm 1$ for brevity) $\psi_{\sigma\tau\mathbf{k}}(\mathbf{r}) = \frac{1}{\sqrt{A}}e^{i\mathbf{k}\cdot\mathbf{r}}\chi_{\sigma\tau}$ where A is the sample area and the valence ($\sigma = v$) and conduction ($\sigma = c$) band eigenspinors $\chi_{\sigma\tau}$ are dominated by, respectively, $|\phi_{v\tau}\rangle$ and $|\phi_{c\tau}\rangle$ near the band edges.[36] In this energy range, the bands are parabolic $\varepsilon_{\sigma\tau\mathbf{k}} = E_{\sigma\tau} \pm \hbar^2k^2/2m^*_\sigma$, where $E_{\sigma\tau} = \pm\Delta/2 + \delta_{v\sigma}\tau\Delta_{\mathrm{SO}}/2$ is the band-edge position (the spin dependence is shown in Fig. 2). The small SO splitting of 2–3 meV in the conduction band of MoS_2[73,74] is here neglected and spin degeneracy is assumed. For the effective masses, we use our calculated DFT values, $m^*_v = 0.59$ and $m^*_c = 0.48$ for 2D MoS_2,[75] which are in good agreement with previously reported values.[26,73,79]

A. Disorder-limited transport

In Boltzmann transport theory, the carrier mobility $\mu_{xx} = \sigma_{xx}/ne$, where σ_{xx} is the conductivity, limited by elastic disorder scattering can be expressed as $\mu_{xx} = e\langle\tau_k\rangle/m^*$, where m^* is the effective mass and τ_k is the total energy-dependent momentum relaxation time given by the sum over contributions from different types of

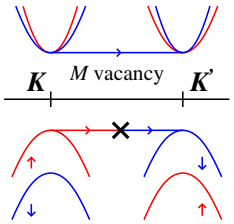

FIG. 2. Band structure and disorder scattering in the K, K' valleys of 2D TMDs. While intravalley scattering is allowed (not shown), intervalley scattering is strongly suppressed by (i) the large spin-orbit splitting in the valence band (for some TMDs also in the conduction band), and (ii) a symmetry-induced selection rule for defects with C_3 symmetry and centered at the M and X sites in both the valence and conduction bands.[42]

disorder, $\tau^{-1} = \sum_i \tau_i^{-1}$. The brackets $\langle\cdot\rangle$ denote the energy-weighted average defined as

$$\langle A\rangle = \frac{1}{n}\int d\varepsilon\ \rho_\sigma(\varepsilon)\varepsilon A(\varepsilon)\left(-\frac{\partial f}{\partial\varepsilon}\right). \tag{2}$$

Here, n is the two-dimensional carrier density, $\rho_\sigma = g_s g_\tau m_\sigma^*/2\pi\hbar^2$ is the constant density of states in 2D, g_s and g_τ are the spin ($g_s = 1, 2$ for $\sigma = v, c$) and valley degeneracy, respectively, $f(\varepsilon) = \{1 + \exp[(\varepsilon-\mu)/k_\mathrm{B}T]\}^{-1}$ is the equilibrium Fermi-Dirac distribution function, and μ is the chemical potential. For a degenerate electron gas, scattering is restricted to a thin shell of width $k_\mathrm{B}T$ around the Fermi level E_F and $\mu_{xx} \approx e\tau(E_F)/m^*$.

For random disorder, the relaxation time due to intra ($\tau = \tau'$) and intervalley ($\tau \neq \tau'$) scattering off defects of type i is in the Born approximation given by

$$\frac{1}{\tau_{i,\sigma\tau}(\varepsilon_\mathbf{k})} = \frac{2\pi}{\hbar} n_i \sum_{\tau'}\int \frac{d\mathbf{k}'}{(2\pi)^2}\,|V^{i,\sigma}_{\mathbf{k}\mathbf{k}'}(\tau,\tau')|^2 \times (1-\cos\theta_{\mathbf{k}\mathbf{k}'})\,\delta(\varepsilon_\mathbf{k}-\varepsilon_{\mathbf{k}'}), \tag{3}$$

where n_i is the disorder density, $V^{i,\sigma}_{\mathbf{k}\mathbf{k}'}(\tau,\tau') = \langle\chi_{\sigma\tau}|\hat{V}_i|\chi_{\sigma\tau'}\rangle$ is the matrix element (in units of eV Å^2) of the defect scattering potential with respect to the electronic states in band σ and with wave vectors $\mathbf{k}, \mathbf{k}'$, and $\theta_{\mathbf{k}\mathbf{k}'}$ is the scattering angle.

Here, we omit spin-flip scattering and limit the discussion to spin-conserving scattering off nonmagnetic defects, $\hat{V}_i \propto \hat{s}_0$. Due to the orthogonality of the K, K' valence-band orbitals, $\langle\phi_{v\tau}|\phi_{v\tau'}\rangle = \delta_{\tau\tau'}$, the valence-band intervalley matrix element is in general suppressed.[36] Recently, we have demonstrated a stricter symmetry-induced selection rule for defects with C_3 symmetry which applies to the intervalley matrix element in both the valence and conduction bands[42] (see also Sec. II B 1 below). As a consequence, intervalley scattering in 2D TMDs is only allowed in the conduction band for metal-centered defects as illustrated in Fig. 2.

Conventionally, point defects such as atomic vacancies are treated as short-range scatterers described by a δ-function scattering potential in real space, $V_i(\mathbf{r}) = V^i_{0,\sigma}\delta(\mathbf{r})$ where $V^i_{0,\sigma}$ is a band-dependent disorder strength. In this case, the matrix element is simply given by

$$V^{i,\sigma}_{\mathbf{k}\mathbf{k}'}(\tau,\tau') = V^i_{0,\sigma}(\tau,\tau'), \tag{4}$$

where the valley dependence accounts for the above-mentioned selection rules. In the Born approximation, this yields a momentum relaxation time, $\tau_i^{-1} = n_i m^* |V^i_{0,\sigma}|^2/\hbar^3$, and mobility, $\mu \sim n^0$, which are independent on the carrier energy and carrier density, respectively. For atomic vacancies in 2D TMDs this approach may break down for two reasons.

First of all, as discussed in the introduction, charging of the vacancy sites in the presence of in-gap states gives rise to two distinct contributions to the scattering potential given, respectively, by (i) a short-range potential (V^i_0) associated with the atomic-scale point defect created by the vacancy, and (ii) a long-range Coulomb potential (V^i_C) due to the charged vacancy site. Here, we assume that the relaxation time for charged vacancies can be obtained as

$$\tau_i^{-1} = \tau_{i,0}^{-1} + \tau_{i,C}^{-1}, \tag{5}$$

where the two relaxation times on the right-hand side account for the above-mentioned contributions to the scattering potential.

Secondly, the Born approximation only applies to *weak* short-range disorder, i.e. when V^i_0 is small (see discussion in Sec. II B 1), and may break down for vacancies. For disorder of arbitrary strength, the *bare* matrix element in Eq. (3) must be replaced with the T matrix, i.e. $V^i_{\mathbf{k}\mathbf{k}'} \to T^i_{\mathbf{k}\mathbf{k}'}(\varepsilon_\mathbf{k})$.[67] The T matrix solves the single-defect problem exactly by taking into account multiple scattering off the individual defects, and is hence *exact* for dilute disorder, i.e. $n_i \ll 1/A_\mathrm{cell}$ where A_cell is the unit-cell area.

In the following subsections, we analyse the scattering properties of atomic vacancies (Mo and S) in 2D TMDs.

B. Short-range potential: V^i_0

Short-range disorder due to atomic point defects often act as strong scattering centers, and must be treated with the T-matrix formalism which describes multiple scattering off the same defect to infinite order in the scattering potential.[67] Here, we combine atomistic calculations with an analytic approach to get a realistic description of the T matrix scattering rate.

1. *Low-energy T-matrix model*

For a general defect characterized by the matrix element $V^{\sigma,i}_{\mathbf{k}\mathbf{k}'}$ of its scattering potential between the Bloch states with wave vectors $\mathbf{k}, \mathbf{k}' \in$ 1st Brillouin zone (BZ),

the T matrix (for a given spin) is given by the integral equation

$$T^{\sigma,i}_{\mathbf{k}\mathbf{k}'}(\varepsilon) = V^{\sigma,i}_{\mathbf{k}\mathbf{k}'} + \int_{\mathrm{BZ}} \frac{d\mathbf{k}_1}{(2\pi)^2} V^{\sigma,i}_{\mathbf{k}\mathbf{k}_1} G^0_{\sigma\mathbf{k}_1}(\varepsilon) T^{\sigma,i}_{\mathbf{k}_1\mathbf{k}'}(\varepsilon), \quad (6)$$

where $G^0_{\sigma\mathbf{k}}(\varepsilon) = (\varepsilon - \varepsilon_{\sigma\mathbf{k}} + i\eta)^{-1}$ is the *bare* Green's function and the integral is over the 1st BZ.

With the bandstructure described by the low-energy model in Eq. (1), we confine the $\mathbf{k}_1$ integral in (6) to the K, K' valleys, i.e. $\int_{\mathrm{BZ}} \frac{d\mathbf{k}}{(2\pi)^2} \to \sum_\tau \int_\tau \frac{d\mathbf{k}}{(2\pi)^2}$, and parametrize the defect matrix element by a band- and valley-dependent disorder strength $V^i_{0,\sigma}$ like in Eq. (4). With this, the T-matrix equation in (6) reduces to a $\mathbf{k}, \mathbf{k}'$-independent algebraic 2×2 matrix equation in the valley indices,

$$\hat{T}^i_\sigma(\varepsilon) = \left[\hat{\tau}_0 - \hat{\bar{G}}_\sigma(\varepsilon)\hat{V}^i_{0,\sigma}\right]^{-1} \hat{V}^i_{0,\sigma}, \quad (7)$$

where $\hat{\bar{G}}_\sigma(\varepsilon) = \mathrm{diag}\left[\bar{G}_{\sigma K}(\varepsilon), \bar{G}_{\sigma K'}(\varepsilon)\right]$ is diagonal with elements given by the $\mathbf{k}$-integrated valley GF, $\bar{G}_{\sigma\tau}(\varepsilon) = \int_\tau \frac{d\mathbf{k}}{(2\pi)^2} G^0_{\sigma\tau\mathbf{k}}(\varepsilon)$, and the diagonal (off-diagonal) elements of $\hat{V}^i_{0,\sigma}$ correspond to intravalley (intervalley) couplings.

In a recent work,[42] we have shown that the $K \leftrightarrow K'$ intervalley coupling due to defects in 2D TMDs with C_3 symmetry is suppressed by a symmetry-induced selection rule, except for M-centered defects where intervalley coupling is possible in the conduction band as illustrated in Fig. 2. As the intra- and intervalley matrix elements for M vacancies are comparable,[42] a single disorder strength can therefore be considered for both M and X vacancies. The defect potential can hence be written

$$\hat{V}^i_{0,\sigma} = V^i_{0,\sigma} \times \begin{cases} \hat{\tau}_0 + \hat{\tau}_x, & \sigma = c,\, i = M \\ \\ \hat{\tau}_0, & \text{otherwise,} \end{cases} \quad (8)$$

which captures the defect and band dependent suppression of the intervalley coupling described above.

With the form of the defect potential in (8), the T matrix in (7) simplifies considerably. For the two cases in (8), we get

$$\hat{T}^i_\sigma(\varepsilon) = \begin{cases} T^i_{cK}(\varepsilon)(\hat{\tau}_0 + \hat{\tau}_x) \\ \\ T^i_{\sigma K}(\varepsilon)\frac{(\hat{\tau}_0 + \hat{\tau}_z)}{2} + T^i_{\sigma K'}(\varepsilon)\frac{(\hat{\tau}_0 - \hat{\tau}_z)}{2}, \end{cases} \quad (9)$$

where

$$T^i_{\sigma\tau}(\varepsilon) = \frac{V^i_{0,\sigma}}{1 - g_{\sigma i} V^i_{0,\sigma} \bar{G}_{\sigma\tau}(\varepsilon)}, \quad (10)$$

is the band and valley dependent T matrix with $g_{\sigma i}$ denoting a valley multiplication factor given by the number of inequivalent valleys coupled by the defect type i, i.e. $g_{cM} = 2$ and $g_{\sigma i} = 1$ otherwise. For the parabolic bands in the K, K' valleys, the $\mathbf{k}$-integrated Green's function $\bar{G}_{\sigma\tau}$ for $\sigma = c, v$ becomes

$$\bar{G}_{\sigma\tau}(\varepsilon) = \pm\bar{\rho}_\sigma \ln\frac{|\varepsilon - E_{\sigma\tau}|}{|\varepsilon - E_{\sigma\tau} \mp \Lambda|} - i\pi\bar{\rho}_\sigma\theta(\varepsilon \mp E_{\sigma\tau}), \quad (11)$$

where $\bar{\rho}_\sigma = m^*_\sigma/2\pi\hbar^2$ is the density of states excluding spin and valley degeneracy, $E_{\sigma\tau}$ is the valley (and spin) dependent band extrema, and Λ is an ultraviolet cut-off to be determined below. Note that due to the neglected spin-orbit splitting in the conduction band, i.e. $E_{cK} = E_{cK'}$, the elements of the T matrix in the upper equation in Eq. (9) become independent on the valley index.

Via the optical theorem,[66,67] $T^i_{\sigma\tau}(\varepsilon)$ in Eq. (10) can be identified as the scattering amplitude in the T-matrix approximation. Together with Eq. (11), the formal condition for disorder to be weak (strong) thus becomes $V^i_{0,\sigma}\bar{\rho}_\sigma \ll 1$ ($\gg 1$). In monolayer MoS_2 $\bar{\rho}_\sigma \approx m^*_\sigma \times 0.02\ \mathrm{eV}^{-1}\mathrm{\AA}^{-2}$, implying that $V^i_{0,\sigma} \gg$ / $\ll 100\ \mathrm{eV\,\AA}^2$ corresponds to strong/weak disorder. For weak disorder, the Born approximation for the scattering amplitude, $T^i_\sigma(\varepsilon) \approx V^i_{0,\sigma}$, is recovered, whereas the T matrix becomes independent on the disorder potential, $T^i_\sigma(\varepsilon) \approx -1/\bar{G}_\sigma(\varepsilon)$, for strong disorder in the *unitary* limit, $V^i_0 \to \infty$. In the *intermediate* regime, the T matrix should also be considered as it gives rise to a nonnegligible renormalization of the Born scattering amplitude.

The T-matrix renormalization of the Born scattering amplitude manifests itself in an inherent energy dependence of the scattering rate. For the T-matrix in Eq. (10), the inverse momentum relaxation time in Eq. (3) becomes,

$$\frac{1}{\tau_{i,\sigma\tau}(\varepsilon)} = \frac{2\pi}{\hbar}\frac{n_i g_{\sigma i}\bar{\rho}_\sigma |V^i_{0,\sigma}|^2}{\left(1 \mp g_{\sigma i}\bar{\rho}_\sigma V^i_{0,\sigma} \ln\frac{|\varepsilon - E_{\sigma\tau}|}{\Lambda}\right)^2 + \left(\pi g_{\sigma i}\bar{\rho}_\sigma V^i_{0,\sigma}\right)^2}, \quad (12)$$

which for the constant defect potentials considered here, is identical to the quantum scattering rate related to the imaginary part of the T matrix [see Eq. (13) below], and given by Eq. (3) with the replacement $(1 - \cos\theta_{\mathbf{k}\mathbf{k}'}) \to 1$. Thus $\tau^{-1}_{i,\sigma\tau}(\varepsilon) = -\frac{2}{\hbar} n_i \mathrm{Im} T^i_{\sigma\tau}(\varepsilon) = \frac{2\pi}{\hbar} n_i g_{\sigma i}\bar{\rho}_\sigma |T^i_{\sigma\tau}(\varepsilon)|^2$ where the factor $g_{\sigma i}\bar{\rho}_\sigma$ stems from the $\mathbf{k}'$ integral in Eq. (3).

Figure 3 shows the energy dependence of the inverse relaxation time in Eq. (12) (full lines) in terms of $-\mathrm{Im}T^i_{\sigma\tau}(\varepsilon)$ for parameters corresponding to Mo and S vacancies in MoS_2 (see Sec. II B 2 below). The characteristic behavior of the scattering rate which increases away from the band edge where it drops sharply, can be traced back to $\bar{G}_\sigma$ in (11) which diverges for $|\varepsilon - E_\sigma| \to 0$ due to the logarithm in its real part. This behavior is inherent to *intermediate* and *strong* short-range disorder, such as, e.g., vacancies and point defects, in 2D materials with parabolic bands, and in stark contrast to the constant relaxation time in the Born approximation, $\tau^{-1}_{i,\sigma\tau} \approx \frac{2\pi}{\hbar} n_i g_{\sigma i}\bar{\rho}_\sigma |V^i_{0,\sigma}|^2$, which is recovered for *weak* disorder.

Also, the above is in contrast to the situation for vacancies in graphene where the scattering rate is predicted to have a nonmonotonic energy dependence due to resonance scattering off quasibound defect states in the vicinity of the Dirac point.[80–84]

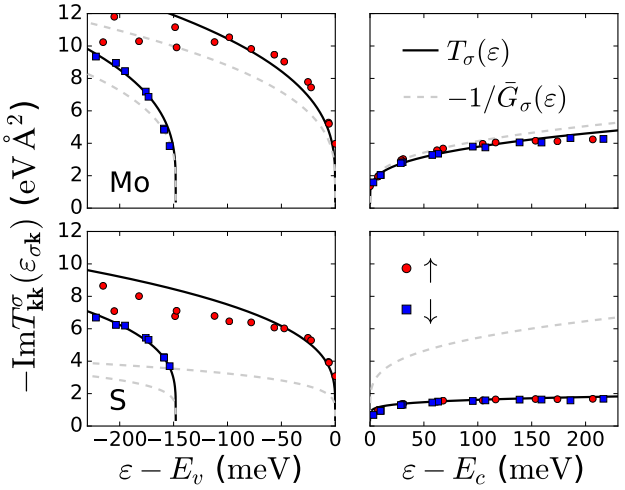

FIG. 3. Imaginary part of the on-shell T matrix as a function of energy in the K valley for the valence ($\sigma = v$, left) and conduction ($\sigma = c$, right) band, and Mo (top) and S (bottom) vacancies. The energy is measured with respect to the band edges E_σ. The symbols show the T matrix obtained with the atomistic DFT method in Ref. 84 (along the path Γ-K-M in the BZ sampled with 135×135 $\mathbf{k}$ points). The solid (dashed) lines show the analytic T matrix in Eq. (10) (unitary limit) with the parameters fitted to the atomistic results as described in Sec. II B 2 (see also Tab. I). Due to the large spin-orbit splitting in valence band, only spin-up points appear at low energies $|\varepsilon - E_v| < \Delta_{\mathrm{SO}}$ where $\Delta_{\mathrm{SO}} = 148$ meV in 2D MoS_2.[72]

	Valence band	Conduction band
Mo vacancy	$V^i_{0,\sigma} = 145\,\mathrm{eV\,Å}^2$	$V^i_{0,\sigma} = 155\,\mathrm{eV\,Å}^2$
	$\Lambda = 8$ eV	$\Lambda = 20$ eV
	$g_{\sigma i} = 1$	$g_{\sigma i} = 2$
S vacancy	$V^i_{0,\sigma} = 24\,\mathrm{eV\,Å}^2$	$V^i_{0,\sigma} = 15\,\mathrm{eV\,Å}^2$
	$\Lambda = 400$ eV	$\Lambda = 100$ eV
	$g_{\sigma i} = 1$	$g_{\sigma i} = 1$

TABLE I. Effective disorder parameters for the analytic T-matrix model in Eq. (10) for Mo and S vacancies in MoS_2. The disorder strengths $V^i_{0,\sigma}$ are fixed to the value of the atomistic DFT matrix elements in Ref. 84, while the energy cutoff is treated as a free parameter in order to fit the atomistic results in Fig. 3 with the analytic model (see Sec. II B 2 for details).

2. *Effective disorder parameters for vacancies*

To determine the T-matrix parameters for Mo and S vacancies which enter Eq. (10), we have used the atomistic method outlined in Refs. 42 and 84 to calculate the T matrix for atomic vacancies in 2D MoS_2 based on Eq. (6) with DFT inputs for the band structure (including spin-orbit interaction) and defect matrix elements sampled in the entire BZ.[75]

In order to quantify our atomistic calculations, we consider the quasiparticle scattering rate $\tau^{-1}_{i,\sigma\mathbf{k}} = \gamma^i_{\sigma\mathbf{k}}/\hbar$, where

$$\gamma^i_{\sigma\mathbf{k}} = -2\mathrm{Im}\,\Sigma^i_{\sigma\mathbf{k}}(\varepsilon_{\sigma\mathbf{k}}) = -2n_i \mathrm{Im}\,T^{\sigma,i}_{\mathbf{kk}}(\varepsilon_{\sigma\mathbf{k}}), \qquad (13)$$

is the lifetime broadening given by the imaginary part of the on-shell ($\varepsilon = \varepsilon_{\sigma\mathbf{k}}$) T-matrix self-energy $\Sigma^i_{\sigma\mathbf{k}} = n_i T^{\sigma,i}_{\mathbf{kk}}$ of the disorder-averaged Green's function.[66,67]

Figure 3 shows the imaginary part of the calculated on-shell T matrix for Mo (top) and S (bottom) vacancies[42,84] as a function energy in the K valley of the valence (left) and conduction (right) band. The red dots and blue squares correspond to the T-matrix for the spin-orbit split spin up and down bands, respectively. In the plots for the valence band, the offset in energy between the red dots and blue squares is due to the large spin-orbit splitting between the spin up and down bands (~ 148 meV) in the K, K' valleys. In the conduction band, the small spin-orbit splitting of $\sim$ 2–3 meV is hardly discernible, and the imaginary part of the T matrix is almost identical for the spin up and down bands. The T-matrix results in Fig. 3 can be converted to a lifetime broadening via Eq. (13), and correspond to a broadening of the order of $\gamma^i_{\sigma\mathbf{k}} \sim 0.01$–$0.1$ meV for a disorder density of $n_i = 10^{11}\,\mathrm{cm}^{-2}$. Furthermore, the atomistic T-matrix results confirm the characteristic energy dependence of the lifetime broadening, or scattering rate, predicted by Eq. (12).

The T-matrix parameters for vacancies are obtained by fitting the analytic expression (10) to the atomistic T matrix in Fig. 3 [we fit the imaginary parts to achieve an optimal description of the scattering rate, cf. Eq. (13)]. In the fitting procedure, we first fix the disorder strength $V^i_{0,\sigma}$ to the value of the atomistic matrix elements $V^{\sigma,i}_{\mathbf{kk}'}$ at the K, K' points (see Refs. 42 and 84), and treat the ultraviolet cutoff Λ as a fitting parameter. This is justified as Λ does not have an immediate physical interpretation in the low-energy T-matrix model. Instead, it should be regarded as an effective parameter which compensates for approximating in Eq. (6) (i) the band structure in the full BZ with parabolic bands in the K, K' valleys, and (ii) the defect matrix element by a constant disorder strength.

The resulting fits are shown with solid lines (the dashed lines show the unitary limit) in Fig. 3, and are seen to match the atomistic calculations almost perfectly, in particular at energies near the band edges relevant for transport. The corresponding fitting parameters are summarized in Table I.

As witnessed by Fig. 3, the T matrix is highly dependent on the band. This is due to the ± 1 factor in front of the real part of $\bar{G}$ in Eq. (11), which even for an electron-hole symmetric bandstructure gives rise to different scattering rates for electrons and holes [cf. Eq. (12)]. For $V^i_0 > 0$ (the reverse holds for $V^i_0 < 0$), this leads to a hole scattering rate which is larger than the electron scattering rate as seen in Fig. 3. For the same reason, the electron and holes rates are, respectively, larger and smaller than the rate for unitary scattering.

Finally, we note that the T-matrix results in Fig. (3) correspond to a significant renormalization of the Born scattering amplitude given by the bare disorder strengths in Tab. I. From the numbers in Fig. 3, the T-matrix scattering amplitudes are found to be up to an order of magnitude *smaller* than the Born scattering amplitudes. The renormalization is most pronounced for Mo vacancies which are strong (almost unitary) scatterers, and still noticeable for the weaker S vacancies. As the scattering rate depends on the square of the scattering amplitude, the Born approximation therefore severely overestimates the scattering rate.

To summarize, the strong T-matrix renormalization of the Born scattering amplitude results in (i) the characteristic energy dependence of the scattering rates in Fig. 3, as well as (ii) a significant reduction of the scattering rate relative to the Born result. These findings points to a concomitant breakdown of the Born approximation for atomic-vacancy scattering in 2D TMDs.

C. Long-range Coulomb potential: V_C^i

The relaxation time in Eq. (5) due to trapped charges in the in-gap states is governed by a long-range Coulomb potential. Due to the localized nature of the in-gap states, this can be approximated by the screened Coulomb potential from a point charge located at the vacancy site, and the matrix element becomes

$$V_C^i(q) = \frac{e^2}{2\epsilon_0 q \epsilon(q)}. \tag{14}$$

where $\epsilon(q) \equiv \epsilon(q, T, \mu)$ is the static dielectric function of the 2D material which includes both intra and interband screening as discussed in further detail in Sec. II C 1 below.

For scattering off the long-range Coulomb potential, we use the Born approximation which is justified due to the screening of the Coulomb potential.[30,31,68,85,86] For a degenerate 2DEG, the dielectric function is given by $\epsilon(q) = \kappa(1 + q_{\rm TF}/q)$, $q < 2k_F$, where $q_{\rm TF} = \frac{g_s g_v e^2 m^*}{4\pi\epsilon_0\kappa\hbar^2}$ is the Thomas-Fermi (TF) wave vector and κ is a background dielectric constant. In 2D TMDs, $q_{\rm TF} \sim \pi/a \gg k_F$, where a is the lattice constant, implying that carrier screening is very efficient. This changes qualitatively the $1/q$ dependence of the unscreened Coulomb potential, with the screened Coulomb matrix element in (14) becoming

$$V_C^i(q) \approx \frac{e^2}{2\epsilon_0 q_{\rm TF}} = \frac{2\pi\hbar^2}{g_s g_v m^*} \equiv V_0^C, \quad q < 2k_F, \tag{15}$$

which is independent on q, and thus resembles short-range disorder with an *effective* disorder strength V_0^C. For $q > 2k_F$, the screening efficiency is reduced and the unscreened $1/q$ potential is recovered. In 2D MoS_2, the effective disorder strengths in the valence and conduction bands are $V_{0,v}^C \approx 41$ eV Å^2 and $V_{0,c}^C \approx 25$ eV Å^2, respectively.

In passing, we note that scattering off an *unscreened* 2D Coulomb potential was studied with a partial-wave analysis (which is equivalent to a T-matrix treatment) in Ref. 87. However, as it has been shown in numerous works,[30,31,68,85,86] it is important to take into account screening for a correct description of the density and temperature dependence of the low-temperature conductivities in 2D systems.

1. Dielectric function

The long-wavelength dielectric function of a doped 2D semiconductor has two contributions: the first is due to the gate-induced *extrinsic* carriers which is normally accounted for in transport studies, and the second from the *intrinsic* screening associated with virtual electron-hole (eh) pair excitation between the valence and conduction bands. Contrary to 3D bulk systems where the latter is well described by the dielectric constant of the material, intrinsic screening in 2D semiconductors is strongly q dependent.[88,89]

The total dielectric function thus becomes

$$\epsilon(q, T, \mu) = 1 - V(q)\chi_{\rm ext}(q, T, \mu) - V(q)\chi_{\rm int}(q) \tag{16}$$

where $V(q) = e^2/2\epsilon_0 q$ is the 2D Fourier transform of the Coulomb interaction and $\chi_{\rm ext}$ ($\chi_{\rm int}$) is the polarizability due to intraband (interband) eh-pair processes involving *extrinsic* (*intrinsic*) carriers. Dielectric screening from the environment is included with the replacements $\epsilon \to \kappa\epsilon$ and $V \to V/\kappa$, where $\kappa = 4.1$ is an effective background dielectric constant for encapsulation in h-BN.[31]

The screening from the *extrinsic* carriers in the valence/conduction band is described with finite-temperature RPA theory where the static polarizability at finite temperatures is given by[90,91]

$$\chi_{\rm ext}(q, T, \mu) = \int_0^\infty d\mu' \, \frac{\chi_{\rm ext}(q, 0, \mu')}{4k_{\rm B}T\cosh^2\frac{\mu-\mu'}{2k_{\rm B}T}}. \tag{17}$$

Here, $\chi_{\rm ext}(q, 0, \mu)$ is the zero-temperature polarizability and the integral is evaluated following Ref. 92. For a degenerate 2DEG, Eq. (17) yields the above-mentioned TF result for the extrinsic screening. In the nondegenerate regime, extrinsic carrier screening is described by Debye-Hückel theory and is strongly reduced. Thus, the strength of the Coulomb potential increases dramatically, and the transport is expected to become dominated by Coulomb-disorder scattering at low carrier density and high temperature.

For the intrinsic screening due to interband eh-pair excitations between the valence and conduction bands, we use the dielectric function[88,89]

$$\begin{aligned}\epsilon_{\rm int}(q) &= 1 - \frac{e^2}{2\epsilon_0 q}\chi_{\rm int}(q) \\ &= 1 + \alpha q,\end{aligned} \tag{18}$$

which is valid in the long-wavelength limit and where α is given by the interband polarizability $\chi_{\rm int}(q) \propto q^2$, and $\alpha \approx 40$ Å for MoS_2.[93,94] Note that the intrinsic screening vanishes, $\epsilon_{\rm int} \to 1$, for $q \to 0$ in 2D semiconductors. As it originates from eh-pair excitations between bands separated by a large band gap, the intrinsic screening is not expected to depend on temperature.

2. Extrinsic vs intrinsic screening

The dielectric function in Eq. (16) is similar to the one in gated graphene.[95] However, due the sizeable band gaps in 2D TMDs, *intrinsic* screening is much weaker than in graphene, and the long-wavelength dielectric function is dominated by intraband processes involving *extrinsic* carriers.

Already from the q dependence of the polarizabilities it is clear that extrinsic screening dominates the total dielectric function in Eq. (16) in the long-wavelength limit. For a degenerate carrier distribution, the wave vector q^* at which the two screening mechanisms contribute equally to the total dielectric function can be estimated by comparing the products of the Coulomb interaction and the polarizabilities,

$$q_{\rm TF}/q^* = \alpha q^* \quad \to \quad q^* = \sqrt{q_{\rm TF}/\alpha}. \tag{19}$$

For monolayer MoS_2, we estimate $q^* \approx 0.3\,\pi/a$ based on the conduction-band TF wave vector. Thus, extrinsic screening dominates at temperatures where the scattering wave vector is limited by $q < 2k_F \ll q^*$, whereas at (i) high temperatures $T \gg T_F$ where extrinsic carrier screening is reduced, and (ii) high carrier densities where k_F becomes appreciable compared to q^*, intrinsic screening becomes important.

III. RESULTS

In the following, we present our results for the density, $\mu \sim n^\alpha$, and temperature, $\mu \sim T^{-\gamma}$, dependencies of the mobility limited by atomic vacancies. As the inverse relaxation time scales directly with the disorder density, we restrict here the discussion to $n_{\rm dis} = 10^{11}$ cm^{-2} which corresponds to a dilute concentration ($c_{\rm dis} \approx 0.01\,\%$) of defects.

From our considerations in the previous section, we anticipate a density scaling of the mobility with (i) $\alpha < 0$ if the short-range potential dominates as the scattering rate increases with the electron and hole energies [cf. Fig. 3 and Eq. (12)], and (ii) $\alpha \gtrsim 0$ if the Coulomb potential dominates.[85,86]

A. Charged vacancies: Coulomb-disorder dominated transport

In Fig. 4 we show the density and temperature dependence of the mobility limited by *charged* vacancies. As we explain below, the results for charged Mo and S vacancies are almost identical, hence only the results for S vacancies are shown. The scaling exponents $\alpha = d\log\mu/d\log n$ and $\gamma = -d\log\mu/d\log T$ are shown in the bottom panels. To emphasize effect of the intrinsic interband screening, we show the results both with (full lines) and without (dashed lines; $\epsilon_{\rm int} = 1$) intrinsic screening, and the dots indicate the densities and temperatures where the Fermi temperature is equal to the actual temperature, $T = T_F$, and hence mark the quantum-classical crossover between the degenerate ($T < T_F$) and nondegenerate ($T > T_F$) regimes.

Overall, the mobilities limited by charged S vacancies show a strong density and temperature dependence with $\alpha > 0$ and $\gamma > 0$, except at high temperatures and low densities where $\gamma < 0$. These observations indicate that the vacancy-independent Coulomb potential scattering dominates the inverse relaxation time for charged vacancies, thus resulting in almost identical mobilities for charged Mo and S vacancies. Based on the observations regarding the energy dependence of the relaxation time in Eq. 12, a $\alpha < 0$ density scaling would have been expected if the short-range potential was dominating.

This is also consistent with the observed strong temperature dependence of the mobility which stems from the temperature-dependent screening of the Coulomb potential. Moving from the quantum-classical crossover into the nondegenerate low-density/high-temperature regimes, the strength of the Coulomb potential increases dramatically due to a strong reduction in the efficiency of extrinsic carrier screening. In turn, this leads to a pronounced reduction of the mobility of up to two orders of magnitude.

The effect of intrinsic screening on the Coulomb potential is evident at high temperatures $T > T_F$ where it becomes comparable to extrinsic screening. Here, it gives rise to an unusual upturn in the mobility with increasing temperature (compare full and dashed lines). Also, at high densities the mobilities show a pronounced upturn with increasing density. This is again due to the intrinsic screening which becomes stronger with increasing density (k_F) due to its linear q dependence in (18). Overall, the differences between the full and dashed lines show that intrinsic screening gives rise to a significant boost of the mobility in the nondegenerate regime and for high densities in the degenerate regime.

Finally, we note that the hole mobilities are in general lower than the electron mobilities in the degenerate regime. This can be attributed to the lack of spin degeneracy in the valence band which results in a weaker screening of Coulomb scattering for holes (cf. Sec. II C).

The density and temperature range where the pronounced screening-induced change in the mobilities in

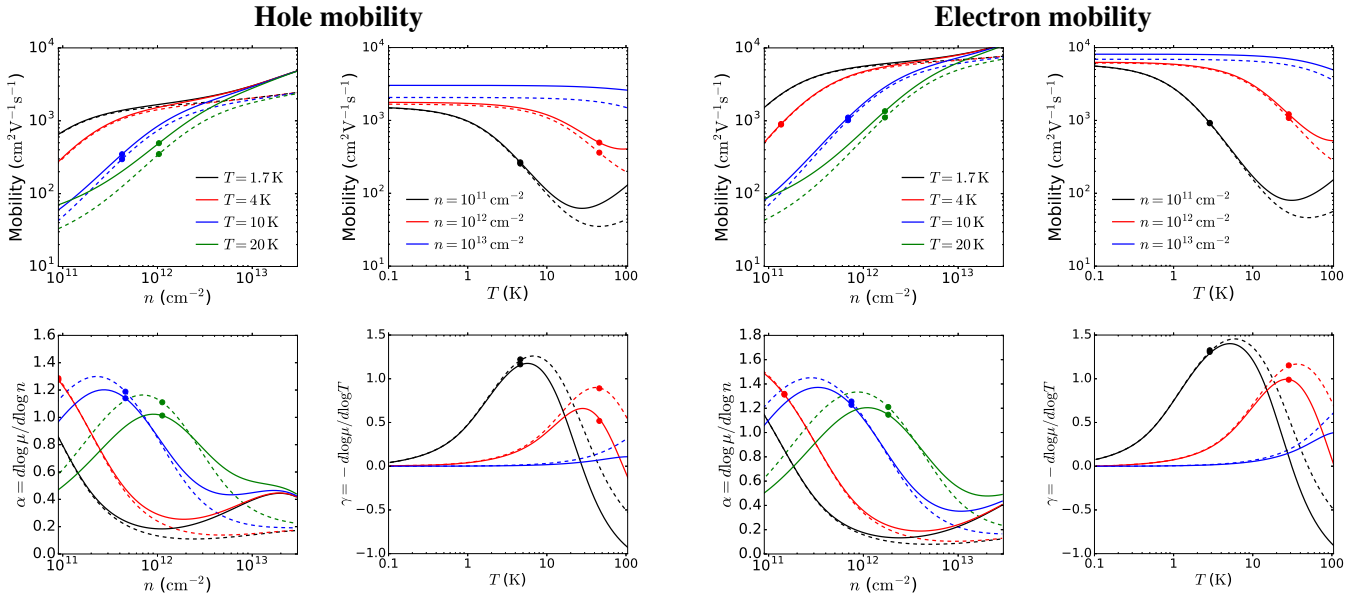

FIG. 4. Hole and electron mobilities limited by *charged* S vacancies. The plots show the hole (left) and electron (right) mobilities vs carrier density and temperature for a disorder density of $n_S = 10^{11}$ cm^{-2}. The corresponding density, $\alpha = d\log\mu/d\log n$, and temperature, $\gamma = -d\log\mu/d\log T$, exponents of the mobilities are shown in the lower row. The weak dashed lines show the mobility in the absence of intrinsic screening. The dots (•) indicate the temperatures and densities where $T = T_F$.

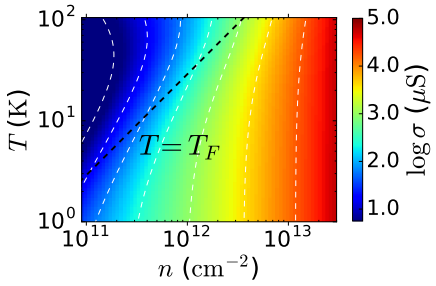

FIG. 5. Transport diagram for n-type 2D MoS_2 showing the conductivity σ limited by *charged* S vacancies ($n_S = 10^{11}$ cm^{-2}) as a function of carrier density n and temperature T.

Fig. 4 takes place, is summarized in the transport diagram shown for the S-vacancy limited conductivity in n-type MoS_2 in Fig. 5. The diagram shows the conductivity $\sigma = e^2 n\langle\tau\rangle/m^*$ (here $\log\sigma$) in the (n, T) plane and the black dashed line indicates the quantum-classical crossover at $T = T_F$. As is evident, the crossover takes place at experimentally easily accessible densities and temperatures.

The quantum-classical crossover is clearly visible in the conductivity data. In the degenerate high-density regime ($T \ll T_F$), the conductivity scales as $\sigma \sim n$ and is almost independent on temperature due to the effective short-range nature of the Coulomb potential in Eq. (15) caused by carrier screening. At $T \gtrsim T_F$, the conductivity acquires a stronger density and temperature dependence due to the reduced screening of the Coulomb potential.

B. Neutral vacancies: Short-range disorder limited transport

In this section, we consider the situation where the vacancies remain neutral in doped samples. This is expected to occur in 2D TMDs where vacancies do not introduce occupied in-gap states (e.g., X = S, Se vacancies in WX_2[55,65]), implying that the vacancy will remain overall neutral in p-doped samples and only the short-range contribution to the relaxation time in Eq. (5) remains.

To demonstrate the impact on the hole mobility in TMDs where the above-mentioned situation is realized, we show in Fig. 6 the hole mobility in MoS_2 limited by *neutral* S vacancies at different temperatures. The dashed line shows the zero-temperature mobility $\mu = e\tau_{i,\sigma}(E_F)/m^*_\sigma$ with the relaxation time obtained from Eq. (12). As the semiconducting 2D TMDs have similar valence band structure, only minor quantitative changes are expected for hole mobility limited by *neutral* M and X vacancies in other TMDs.

First of all, we note that the mobilities are more than an order of magnitude higher than the ones in Fig. 4 limited by charged vacancies, except at the highest carrier densities where they become comparable. The fact that the mobilities are higher for neutral vacancies, is not surprising because the Coulomb potential completely dominates the short-range potential for scattering off charged vacancies. As we had anticipated from the scattering rates deduced from Fig. 3, the mobilities in Fig. 6 limited alone by the short-range potential due to neutral vacancies, decrease with increasing carrier density. This

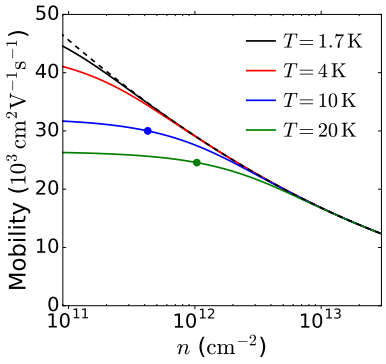

FIG. 6. Hole mobility in 2D MoS_2 limited by *neutral* S vacancies, $n_S = 10^{11}$ cm^{-2}, at different temperatures. The dashed line shows the zero-temperature mobility $\mu_{xx} = e\tau_{i,\sigma}(E_F)/m^*_\sigma$ with $\tau_{i,\sigma}$ given by its T-matrix form in Eq. (12).

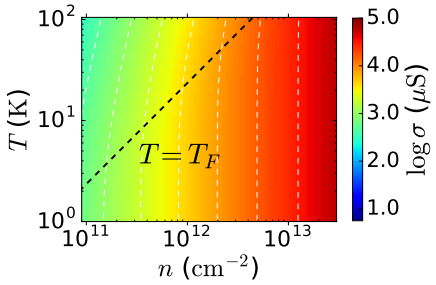

FIG. 7. Transport diagram for p-type 2D MoS_2 showing the conductivity σ limited by *neutral* neutral S vacancies ($n_S = 10^{11}$ cm^{-2}) as a function of carrier density n and temperature T.

rather unusual density dependence of the mobility is a direct consequence of the T-matrix induced renormalization of the scattering amplitude. At low densities, the decreasing temperature dependence of the mobility stems from the energy average of the relaxation time in Eq. (2), which with increasing temperature probes the increasing energy dependence of the scattering rate at higher energies. The resulting reduction in the mobility is, however, much smaller than the sceening-related reduction observed for charged vacancies.

The qualitative difference between the screening-induced and T-matrix induced density and temperature dependencies of the mobility emerges clearly from the transport diagrams for charged and neutral vacancies in Figs. 5 and 7, respectively. While in the latter case, the conductivity $\sigma \sim n^\alpha$ scales roughly as $\alpha \approx 1$ on both sides of the quantum-classical crossover, the screening-induced density dependence of the scattering rate in the former case results in a stronger $\alpha \approx 2$ behavior in the nondegenerate regime at $T \gtrsim T_F$.

These qualitative differences in the transport characteristics allow to clearly distinguish Coulomb-disorder limited transport from short-range limited transport due to, e.g., charged and neutral vacancies, respectively.

IV. DISCUSSION

Reported experimental low-temperature mobilities in 2D TMDs have thus far been rather low,[13,14,16,17,19,62,63] and have only recently exceeded $\sim$1000 cm^{-2} V^{-1} s^{-1}.[11,22–25] This is still slightly lower than our calculated mobilities limited by charged vacancies and much lower than the calculated mobilities limited by neutral vacancies. This indicates that the concentration of vacancies in experimental samples could be higher than $n_{\rm dis} = 10^{11}$ cm^{-2} used here. Several reports of high concentrations of S vacancies[16,59] suggest that this is indeed a likely reason for the low experimental mobilities. Only recently have defect densities of $n_{\rm dis} \sim 10^{11}$ cm^{-2} been demonstrated.[47] However, experimental transport properties of such high-quality TMDs have so far not been reported.

The often observed strong metallic temperature and density dependence of experimental low-temperature mobilities[13,14,16,17,19,62,63] resemble best our results for charged vacancies. This indicates that a combination short-range and Coulomb-disorder scattering is limiting the low-temperature mobility in 2D TMDs. As we here suggest, vacancies may be the source of both short-range and Coulomb disorder scattering. Hence, there is no need to introduce additional Coulomb disorder[30,31] (e.g., charged impurities in the substrate) in order to account for the metallic transport behavior.

V. CONCLUSIONS

In conclusion, we have studied the effect of atomic vacancies on carrier scattering and transport in p- and n-type monolayer MoS_2. Due to the presence of both filled and empty vacancy-induced in-gap states, the vacancies can be expected to become *charged* in p- and n-doped MoS_2, and thereby give rise to both short-range and Coulomb disorder scattering. The situation is similar for vacancies in many other 2D TMDs, but cases lacking filled in-gap states have been reported, implying that the vacancy remain *neutral* in the p-doped material.

Studying the short-range scattering properties of vacancies with the T-matrix formalism, we show that multiple scattering gives rise to a strong renormalization of the Born scattering amplitude, which results in a pronounced reduction as well as a characteristic energy dependence of the scattering rate. As a result, the Coulomb contribution to the scattering potential for *charged* vacancies by far dominates carrier scattering. This results in a strong screening-induced temperature and density dependence of the mobility in 2D TMDs hosting charged vacancies. For TMDs with *neutral* vacancies the mobility is significantly higher and shows an unusual behavior with a decreasing density dependence. Thus, TMDs in which vacancies remain neutral in the doped material are better candidates for high-mobility devices.

ACKNOWLEDGMENTS

K.K. acknowledges support from the Carlsberg Foundation and the European Union's Horizon 2020 research and innovation program under the Marie Sklodowska-Curie Grant Agreement No. 713683 (COFUNDfellowsDTU). T.L. acknowledges partial support from NSF ECCS-1542202. The Center for Nanostructured Graphene (CNG) is sponsored by the Danish National Research Foundation, Project DNRF103.

* kkaa@dtu.dk

[1] K. F. Mak, C. Lee, J. Hone, J. Shan, and T. F. Heinz, "Atomically thin MoS_2: A new direct-gap semiconductor," Phys. Rev. Lett. **105**, 136805 (2010).

[2] B. Radisavljevic, A. Radenovic, J. Brivio, V. Giacometti, and A. Kis, "Single-layer MoS_2 transistors," Nature Nano. **6**, 147 (2011).

[3] T. Korn, S. Heydrich, M. Hirmer, J. Schmutzler, and C. Schüller, "Low-temperature photocarrier dynamics in monolayer MoS_2," Appl. Phys. Lett. **99**, 102109 (2011).

[4] Phaedon Avouris, Tony F Heinz, and Tony Low, *2D Materials* (Cambridge University Press, 2017).

[5] D. Xiao, G.-B. Liu, W. Feng, X. Xu, and W. Yao, "Coupled spin and valley physics in monolayers of MoS_2 and other group-VI dichalcogenides," Phys. Rev. Lett. **108**, 196802 (2012).

[6] X. Xu W. Yao, D. Xiao, and T. F. Heinz, "Spin and pseudospins in layered transition metal dichalcogenides," Nature Phys. **10**, 343 (2014).

[7] A. Kormányos, V. Zólyomi, N. D. Drummond, and G. Burkard, "Spin-orbit coupling, quantum dots, and qubits in monolayer transition metal dichalcogenides," Phys. Rev. X **4**, 011034 (2014).

[8] G.-B. Liu, H. Pang, Y. Yao, and W. Yao, "Intervalley coupling by quantum dot confinement potentials in monolayer transition metal dichalcogenides," New J. Phys. **16**, 105011 (2014).

[9] Y. Wu, Q. Tong, G.-B. Liu, H. Yu, and W. Yao, "Spin-valley qubit in nanostructures of monolayer semiconductors: Optical control and hyperfine interaction," Phys. Rev. B **93**, 045313 (2016).

[10] J. Pawlowski, D. Zebrowski, and S. Bednarek, "Valley qubit in gated MoS_2 monolayer quantum dot," Phys. Rev. B **97**, 155412 (2018).

[11] R. Pisoni, Z. Lei, P. Back, M. Eich, H. Overweg, Y. Lee, K. Watanabe, T. Taniguchi, T. Ihn, and K. Ensslin, "Gate-tunable quantum dot in a high quality single layer MoS_2 van der Waals heterostructure," Appl. Phys. Lett. **112**, 123101 (2018).

[12] D. Rhodes, S. H. Chae, R. Ribeiro-Palau, and J. Hone, "Disorder in van der Waals heterostructures of 2D materials," Nature Mat. **18**, 541 (2019).

[13] B. Radisavljevic and A. Kis, "Mobility engineering and a metal-insulator transition in monolayer MoS_2," Nature Mat. **12**, 815 (2013).

[14] B. W. H. Baugher, H. O. H. Churchill, Y. Yang, and P. Jarillo-Herrero, "Intrinsic electronic transport properties of high-quality monolayer and bilayer MoS_2," Nano. Lett. **13**, 4212 (2013).

[15] W. Zhu, T. Low, Y.-H. Lee, H. Wang, D. B. Farmer, J. Kong, F. Xia, and P. Avouris, "Electronic transport and device prospects of monolayer molybdenum disulphide grown by chemical vapour deposition," Nature Commun. **5**, 3087 (2014).

[16] Z. Yu, Y. Pan, Y. Shen, Z. Wang, Z.-Y. Ong, T. Xu, R. Xin, L. Pan, B. Wang, L. Sun, J. Wang, G. Zhang, Y. W. Zhang, Y. Shi, and X. Wang, "Towards intrinsic charge transport in monolayer molybdenum disulfide by defect and interface engineering," Nature Commun. **5**, 5290 (2014).

[17] H. Schmidt, S. Wang, L. Chu, M. Toh, R. Kumar, W. Zhao, A. H. Castro Neto, J. Martin, S. Adam, B. Özyilmaz, and G. Eda, "Transport properties of monolayer MoS_2 grown by chemical vapor deposition," Nano. Lett. **14**, 1909 (2014).

[18] L. Chu, H. Schmidt, J. Pu, S. Wang, B. Özyilmaz, T. Takenobu, and G. Eda, "Charge transport in ion-gated mono-, bi-, and trilayer MoS_2 field effect transistors," Scientific Reports **4**, 7293 (2014).

[19] X. Cui, G.-H. Lee, Y. Duck Kim, G. Arefe, P. Y. Huang, C.-H. Lee, D. A. Chenet, X. Zhang, L. Wang, F. Ye, F. Pizzocchero, B. S. Jessen, K. Watanabe, T. Taniguchi, D. A. Muller, T. Low, P. Kim, and J. Hone, "Multi-terminal transport measurements of MoS_2 using a van der Waals heterostructure device platform," Nature Nano. **10**, 534 (2015).

[20] H. Schmidt, I. Yudhistira, L. Chu, A. H. Castro Neto, B. Özyilmaz, S. Adam, and G. Eda, "Quantum transport and observation of Dyakonov-Perel spin-orbit scattering in monolayer MoS_2," Phys. Rev. Lett. **116**, 046803 (2016).

[21] X. Cui, E.-M. Shih, L. A. Jauregui, S. H. Chae, Y. D. Kim, B. Li, D. Seo, K. Pistunova, J. Yin, J.-H. Park, H.-J. Choi, Y. H. Lee, K. Watanabe, T. Taniguchi, P. Kim, C. R. Dean, and J. C. Hone, "Low-temperature ohmic contact to monolayer MoS_2 by van der Waals bonded Co/h-BN electrodes," Nano. Lett. **17**, 4781 (2017).

[22] B. Fallahazad, H. C. P. Movva, K. Kim, S. Larentis, T. Taniguchi, K. Watanabe, S. K. Banerjee, and E. Tutuc, "Shubnikov-de Haas oscillations of high-mobility holes in monolayer and bilayer WSe_2: Landau level degeneracy, effective mass, and negative compressibility," Phys. Rev. Lett. **116**, 086601 (2016).

[23] M. V. Gustafsson, M. Yankowitz, C. Forsythe, D. Rhodes, K. Watanabe, T. Taniguchi, J. Hone, X. Zhu, and C. R. Dean, "Ambipolar Landau levels and strong band-selective carrier interactions in monolayer WSe_2," Nature Mat. **17**, 411 (2018).

[24] S. Larentis, H. C. P. Movva, B. Fallahazad, K. Kim, A. Behroozi, T. Taniguchi, K. Watanabe, S. K. Banerjee, and E. Tutuc, "Large effective mass and interaction-enhanced Zeeman splitting of K-valley electrons in $MoSe_2$," Phys. Rev. B **97**, 201407(R) (2018).

[25] R. Pisoni, A. Kormányos, M. Brooks, Z. Lei, P. Back, M. Eich, H. Overweg, Y. Lee, P. Rickhaus, K. Watanabe, T. Taniguchi, A. Imamoglu, G. Burkard, T. Ihn, and K. Ensslin, "Interactions and magnetotransport through spin-valley coupled Landau levels in monolayer MoS_2," Phys. Rev. Lett. **121**, 247701 (2018).

[26] K. Kaasbjerg, K. S. Thygesen, and K. W. Jacobsen, "Phonon-limited mobility in MoS_2 from first principles," Phys. Rev. B **85**, 115317 (2012).

[27] K. Kaasbjerg, K. S. Thygesen, and A.-P. Jauho, "Acoustic phonon-limited mobility in two-dimensional MoS_2: Deformation potential and piezoelectric scattering from first principles," Phys. Rev. B **87**, 235312 (2013).

[28] Y. Song and H. Dery, "Transport theory of monolayer transition-metal dichalcogenides through symmetry," Phys. Rev. Lett. **111**, 026601 (2013).

[29] Z Jin, X. Li, J. T. Mullen, and K. W. Kim, "Intrinsic transport properties of electrons and holes in monolayer transition-metal dichalcogenides," Phys. Rev. B **90**, 045422 (2014).

[30] Z.-Y. Ong and M. V. Fischetti, "Mobility enhancement and temperature dependence in top-gated single-layer MoS_2," Phys. Rev. B **88**, 165316 (2013).

[31] N. Ma and D. Jena, "Charge scattering and mobility in atomically thin semiconductors," Phys. Rev. X **4**, 011043 (2014).

[32] M. Ghorbani-Asl, A. N. Enyashin, A. Kuc, G. Seifert, and T. Heine, "Defect-induced conductivity anisotropy in MoS_2 monolayers," Phys. Rev. B **88**, 245440 (2013).

[33] S. Yuan, R. Roldán, M. I. Katsnelson, and F. Guinea, "Effect of point defects on the optical and transport properties of MoS_2 and WS_2," Phys. Rev. B **90**, 041402(R) (2014).

[34] T. Olsen and I. Souza, "Valley Hall effect in disordered monolayer MoS_2 from first principles," Phys. Rev. B **92**, 125146 (2015).

[35] H.-Z. Lu, W. Yao, D. Xiao, and S.-Q. Shen, "Intervalley scattering and localization behaviors of spin-valley coupled dirac fermions," Phys. Rev. Lett. **110**, 016806 (2013).

[36] W.-Y. Shan, H.-Z. Lu, and D. Xiao, "Spin Hall effect in spin-valley coupled monolayers of transition metal dichalcogenides," Phys. Rev. B **88**, 125301 (2013).

[37] M. A. Cazalilla, H. Ochoa, and F. Guinea, "Quantum spin Hall effect in two-dimensional crystals of transition-metal dichalcogenides," Phys. Rev. Lett. **113**, 077201 (2014).

[38] H. Ochoa, F. Finocchiaro, F. Guinea, and V. I. Fal'ko, "Spin-valley relaxation and quantum transport regimes in two-dimensional transition-metal dichalcogenides," Phys. Rev. B **90**, 235429 (2014).

[39] M. Tahir, P. Vasilopoulos, and F. M. Peeters, "Quantum magnetotransport properties of a MoS_2 monolayer," Phys. Rev. B **93**, 035406 (2016).

[40] A. Kormányos, P. Rakyta, and G. Burkard, "Landau levels and Shubnikov-de Haas oscillations in monolayer transition metal dichalcogenide semiconductors," New J. Phys. **17**, 103006 (2015).

[41] S. Ilić, J. S. Meyer, and M. Houzet, "Weak localization in transition metal dichalcogenide monolayers and their heterostructures with graphene," Phys. Rev. B **99**, 205407 (2019).

[42] K. Kaasbjerg, J. H. J. Martiny, T. Low, and A.-P. Jauho, "Symmetry-forbidden intervalley scattering by atomic defects in monolayer transition-metal dichalcogenides," Phys. Rev. B **96**, 241411(R) (2017).

[43] W. Zhou, X. Zou, S. Najmaei, Z. Liu, Y. Shi, J. Kong, J. Lou, P. M. Ajayan, B. I. Yakobson, and J.-C. Idrobo, "Intrinsic structural defects in monolayer molybdenum disulfide," Nano. Lett. **13**, 2615 (2013).

[44] Y.-C. Lin, T. Björkman, H.-P. Komsa, P.-Y. Teng, C.-H. Yeh, F.-S. Huang, K.-H. Lin, J. Jadczak, Y.-S. Huang, P.-W. Chiu, A. V. Krasheninnikov, and K. Suenaga, "Three-fold rotational defects in two-dimensional transition metal dichalcogenides," Nature Commun. **6**, 6736 (2014).

[45] J. Hong, Z. Hu, M. Probert, K. Li, D. Lv, X. Yang, L. Gu, N. Mao, Q. Feng, L. Xie, J. Zhang, D. Wu, Z. Zhang, C. Jin, W. Ji, X. Zhang, J. Yuan, and Z. Zhang, "Exploring atomic defects in molybdenum disulphide monolayers," Nature Commun. **6**, 6293 (2015).

[46] S. Zhang, C.-G. Wang, M.-Y. Li, D. Huang, L.-J. Li, W. Ji, and S. Wu, "Defect structure of localized excitons in a WSe_2 monolayer," Phys. Rev. Lett. **119**, 046101 (2017).

[47] D. Edelberg, D. Rhodes, A. Kerelsky, B. Kim, J. Wang, A. Zangiabadi, C. Kim, A. Abhinandan, J. Ardelean, M. Scully, D. Scullion, L. Embon, R. Zu, Elton J. G. Santos, L. Balicas, C. Marianetti, K. Barmak, X.-Y. Zhu, J. C. Hone, and A. N. Pasupathy, "Approaching the intrinsic limit in transition metal diselenides via point defect control," Nano. Lett. **19**, 4371 (2019).

[48] B. Schuler, D. Y. Qiu, S. Refaely-Abramson, , C. Kastl, C. T. Chen, S. Barja, R. J. Koch, D. F. Ogletree, S. Aloni, A. M. Schwartzberg, J. B. Neaton, S. G. Louie, and A. Weber-Bargioni, "Large spin-orbit splitting of deep in-gap defect states of engineered sulfur vacancies in monolayer WS_2," Phys. Rev. Lett. **123**, 076801 (2019).

[49] H.-P. Komsa, J. Kotakoski, S. Kurasch, O. Lehtinen, U. Kaiser, and A. V. Krasheninnikov, "Two-dimensional transition metal dichalcogenides under electron irradiation: Defect production and doping," Phys. Rev. Lett. **109**, 035503 (2012).

[50] D. Liu, Y. Guo, L. Fang, and J. Robertson, "Sulfur vacancies in monolayer MoS_2 and its electrical contacts," Appl. Phys. Lett. **103**, 183113 (2013).

[51] J.-Y. Noh, H. Kim, and Y.-S. Kim, "Stability and electronic structures of native defects in single-layer MoS_2," Phys. Rev. B **89**, 205417 (2014).

[52] H.-P. Komsa, N. Berseneva, A. V. Krasheninnikov, and R. M. Nieminen, "Charged point defects in the flatland: Accurate formation energy calculations in two-dimensional materials," Phys. Rev. X **4**, 031044 (2014).

[53] A. Carvalho and A. H. Castro Neto, "Donor and acceptor levels in semiconducting transition-metal dichalcogenides," Phys. Rev. B **89**, 081406(R) (2014).

[54] H.-P. Komsa and A. V. Krasheninnikov, "Native defects in bulk and monolayer MoS_2 from first principles," Phys. Rev. B **91**, 125304 (2015).

[55] S. Haldar, H. Vovusha, M. K. Yadav, O. Eriksson, and B. Sanyal, "Systematic study of structural, electronic, and optical properties of atomic-scale defects in the two-dimensional transition metal dichalcogenides MX_2 (M=Mo, W; X=S, Se, Te)," Phys. Rev. B **92**, 235408 (2015).

[56] M. Pandey, F. A. Rasmussen, K. Kuhar, T. Olsen, K. W. Jacobsen, and K. S. Thygesen, "Defect-tolerant monolayer transition metal dichalcogenides," Nano. Lett. **16**, 2234 (2016).

[57] M. A. Khan, M. Erementchouk, J. Hendrickson, and M. N. Leuenberger, "Electronic and optical properties of vacancy defects in single-layer transition metal dichalcogenides," Phys. Rev. B **95**, 245435 (2017).

[58] S. Ghatak, A. N. Pal, and A. Ghosh, "Nature of electronic states in atomically thin MoS_2 field-effect transistors," ACS Nano **5**, 7707 (2011).

[59] H. Qiu, T. Xu, Z. Wang, W. Ren, H. Nan, Z. Ni, Q. Chen, S. Yuan, F. Miao, F. Song, G. Long, Y. Shi, L. Sun, J. Wang, and X. Wang, "Hopping transport

through defect-induced localized states in molybdenum disulphide," Nature Commun. **4**, 2642 (2013).

[60] X. Chen, Z. Wu, S. Xu, L. Wang, R. Huang, Y. Han, W. Ye, W. Xiong, T. Han, G. Long, Y. Wang, Y. He, Y. Cai, P. Sheng, and N. Wang, "Probing the electron states and metal-insulator transition mechanisms in molybdenum disulphide vertical heterostructures," Nature Commun. **6**, 6088 (2014).

[61] E. Ponomarev, Á. Pásztor, A. Waelchli, A. Scarfato, N. Ubrig, C. Renner, and A. F. Morpurgo, "Hole transport in exfoliated monolayer MoS_2," ACS Nano **12**, 2669 (2018).

[62] Y. Cui, R. Xin, Z. Yu, Y. Pan, Z.-Y. Ong, X. Wei, J. Wang, H. Nan, Z. Ni, Y. Wu, T. Chen, Y. Shi, B. Wang, G. Zhang, Y.-W. Zhang, and X. Wang, "High-performance monolayer WS_2 field-effect transistors on high-k dielectrics," Advanced Materials **27**, 5230 (2015).

[63] Z. Yu, Z.-Y. Ong, Y. Pan, Y. Cui, R. Xin, Y. Shi, B. Wang, Y. Wu, T. Chen, Y.-W. Zhang, G. Zhang, and X. Wang, "Realization of room-temperature phonon-limited carrier transport in monolayer MoS_2 by dielectric and carrier screening," Advanced Materials **28**, 547 (2016).

[64] Z. Yu, Z.-Y. Ong, S. Li, J.-B. Xu, G. Zhang, Y.-W. Zhang, Y. Shi, and X. Wang, "Analyzing the carrier mobility in transition-metal dichalcogenide MoS_2 field-effect transistors," Adv. Funct. Mater. **27**, 1604093 (2017).

[65] W.-F. Li, C. Fang, and M. A. van Huis, "Strong spin-orbit splitting and magnetism of point defect states in monolayer WS_2," Phys. Rev. B **94**, 195425 (2016).

[66] J. Rammer, *Quantum Transport Theory* (Perseus Books, 1998).

[67] H. Bruus and K. Flensberg, *Many-body Quantum Theory in Condensed Matter Physics* (Oxford University Press, 2004).

[68] S. Das Sarma and E. H. Hwang, "Screening and transport in 2D semiconductor systems at low temperatures," Scientific Reports **5**, 16655 (2015).

[69] A. Ovchinnikov, A. Allain, Y.-S. Huang, D. Dumcenco, and A. Kis, "Electrical transport properties of single-layer WS_2," ACS Nano **8**, 8174 (2014).

[70] K. F. Mak, K. L. McGill, J. Park, and P. L. McEuen, "The valley Hall effect in MoS_2 transistors," Science **344**, 1489 (2014).

[71] L. Chu, I. Yudhistira, H. Schmidt, T. Chun Wu, S. Adam, and G. Eda, "Phase coherent transport in bilayer and trilayer MoS_2," Phys. Rev. B **XXX**, XXX (2019).

[72] Z. Y. Zhu, Y. C. Cheng, and U. Schwingenschlögl, "Giant spin-orbit-induced spin splitting in two-dimensional transition-metal dichalcogenide semiconductors," Phys. Rev. B **84**, 153402 (2011).

[73] A. Kormányos, V. Zólyomi, N. D. Drummond, P. Rakyta, G. Burkard, and V. I. Fal'ko, "Monolayer MoS_2: Trigonal warping, the Γ valley, and spin-orbit coupling effects," Phys. Rev. B **88**, 045416 (2013).

[74] K. Kośmider, J. W. González, and J. Fernández-Rossier, "Large spin splitting in the conduction band of transition metal dichalcogenide monolayers," Phys. Rev. B **88**, 245436 (2013).

[75] The DFT calculations of the band structure, effective masses, and defect matrix elements have been performed with the electronic structure code GPAW[76–78] within the projector augmented-wave method, using the LDA xc functional and a LCAO double-zeta polarized (DZP) basis set. The defect potentials were obtained using a 11×11 supercell with 10 Å of vacuum between the MoS_2 sheet and the cell boundaries in the vertical direction imposed with Dirichlet boundary conditions in order to avoid spurious interlayer interactions. Lastly, the defect matrix elements and T matrix were calculated on a 135×135 BZ grid using a numerical broadening of $\eta = 10$ meV.

[76] J. J. Mortensen, L. B. Hansen, and K. W. Jacobsen, "Real-space grid implementation of the projector augmented wave method," Phys. Rev. B **71**, 035109 (2005).

[77] A. H. Larsen, M. Vanin, J. J. Mortensen, K. S. Thygesen, and K. W. Jacobsen, "Localized atomic basis set in the projector augmented wave method," Phys. Rev. B **80**, 195112 (2009).

[78] J. Enkovaara *et al.*, "Electronic structure calculations with GPAW: a real-space implementation of the projector augmented-wave method," J. Phys.: Cond. Matt. **22**, 253202 (2010).

[79] T. Cheiwchanchamnangij and W. R. L. Lambrecht, "Quasiparticle band structure calculation of monolayer, bilayer, and bulk MoS_2," Phys. Rev. B **85**, 205302 (2012).

[80] P. M. Ostrovsky, I. V. Gornyi, and A. D. Mirlin, "Electron transport in disordered graphene," Phys. Rev. B **74**, 235443 (2006).

[81] T. Stauber, N. M. R. Peres, and F. Guinea, "Electronic transport in graphene: A semiclassical approach including midgap states," Phys. Rev. B **76**, 205423 (2007).

[82] D. M. Basko, "Resonant low-energy electron scattering on short-range impurities in graphene," Phys. Rev. B **78**, 115432 (2008).

[83] T. O. Wehling, S. Yuan, A. I. Lichtenstein, A. K. Geim, and M. I. Katsnelson, "Resonant scattering by realistic impurities in graphene," Phys. Rev. Lett. **105**, 056802 (2010).

[84] K. Kaasbjerg, "Atomistic T-matrix theory of disordered 2D materials: bound states, spectral properties, quasiparticle scattering and transport," In preparation.

[85] S. Das Sarma and E. H. Hwang, "Universal density scaling of disorder-limited low-temperature conductivity in high-mobility two-dimensional systems," Phys. Rev. B **88**, 035439 (2013).

[86] S. Das Sarma and E. H. Hwang, "Short-range disorder effects on electronic transport in two-dimensional semiconductor structures," Phys. Rev. B **89**, 121413(R) (2014).

[87] Q. g. Lin, "Scattering by a Coulomb field in two dimensions," Am. J. Phys. **65**, 1007 (1997).

[88] P. Cudazzo, I. V. Tokatly, and A. Rubio, "Dielectric screening in two-dimensional insulators: Implications for excitonic and impurity states in graphane," Phys. Rev. B **84**, 085406 (2011).

[89] D. Y. Qiu, F. H. da Jornada, and S. G. Louie, "Screening and many-body effects in two-dimensional crystals: Monolayer MoS_2," Phys. Rev. B **235435**, 93 (2016).

[90] P. F. Maldague, "Many-body corrections to the polarizability of the two-dimensional electron gas," Surf. Sci. **73**, 296 (1978).

[91] T. Ando, A. B. Fowler, and F. Stern, "Electronic properties of two-dimensional systems," Rev. Mod. Phys. **54**, 437 (1982).

[92] K. Flensberg and B. Yu-Kuang Hu, "Plasmon enhancement of Coulomb drag in double-quantum-well systems," Phys. Rev. B **52**, 14796 (1995).

[93] S. Latini, T. Olsen, and K. S. Thygesen, "Excitons in van der Waals heterostructures: The important role of dielectric screening," Phys. Rev. B **92**, 245123 (2015).

[94] T. Olsen, S. Latini, F. Rasmussen, and K. S. Thygesen, "Simple screened Hydrogen model of excitons in two-dimensional materials," Phys. Rev. Lett. **116**, 056401 (2016).

[95] E. H. Hwang and S. Das Sarma, "Dielectric function, screening, and plasmons in two-dimensional graphene," Phys. Rev. B **75**, 205418 (2007).